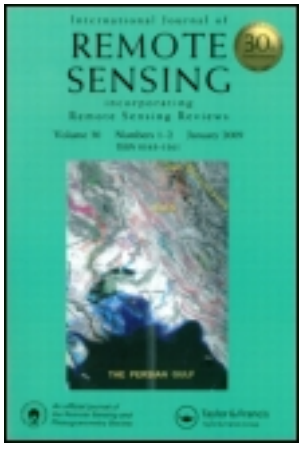

International Journal of Remote Sensing

Publication details, including instructions for authors and subscription information:
http://www.tandfonline.com/loi/tres20

Estimating the coverage of coral reef benthic communities from airborne hyperspectral remote sensing data: multiple discriminant function analysis and linear spectral unmixing

Sarah Hamylton [a b]

[a] Cambridge Coastal Research Unit, Department of Geography, University of Cambridge, Cambridge, CB2 3EN, UK

[b] Darwin College, University of Cambridge, Cambridge, CB3 9EU, UK

Available online: 22 Aug 2011

To cite this article: Sarah Hamylton (2011): Estimating the coverage of coral reef benthic communities from airborne hyperspectral remote sensing data: multiple discriminant function analysis and linear spectral unmixing, International Journal of Remote Sensing, 32:24, 9673-9690

To link to this article: http://dx.doi.org/10.1080/01431161.2011.574162

International Journal of Remote Sensing
Vol. 32, No. 24, 20 December 2011, 9673–9690

Taylor & Francis
Taylor & Francis Group

Estimating the coverage of coral reef benthic communities from airborne hyperspectral remote sensing data: multiple discriminant function analysis and linear spectral unmixing

SARAH HAMYLTON*†‡
†Cambridge Coastal Research Unit, Department of Geography, University of Cambridge, Cambridge CB2 3EN, UK
‡Darwin College, University of Cambridge, Cambridge CB3 9EU, UK

(*Received 19 January 2010; in final form 15 October 2010*)

A staged approach for the application of linear spectral unmixing techniques to airborne hyperspectral remote sensing data of reef communities of the Al Wajh Barrier, Red Sea, is presented. Quantification of the percentage composition of four different reef components (live coral, dead coral, macroalgae and carbonate sand) contained within the ground sampling distance associated with an individual pixel is demonstrated. In the first stage, multiple discriminant function analysis is applied to spectra collected *in situ* to define an optimal subset combination of derivative and raw image wavebands for discriminating reef benthos. In the second phase, unmixing is applied to a similarly reduced subset of pre-processed image data to accurately determine the relative abundance of the reef benthos ($R^2 > 0.7$ for all four components). The result of a phased approach is an increased signal-to-noise ratio for solution of the linear functions and reduction of processing burdens associated with image unmixing.

1. Introduction

Standardized survey protocols are of value to coastal managers because they permit assessment of regional biological diversity and ecological status, allow comparison of status within and between ecoregions and facilitate the detection of change in coastal ecosystem status against established baselines (English *et al*. 1997). Remotely sensed imagery provides an attractive tool for quantitative and systematic monitoring of coral reef health at a broad synoptic scale (e.g. the typical swath width of a remotely sensed image ranges from 500 m to 100 km). Since the 1970s, sensing instruments have increasingly been operated from satellite or airborne platforms to acquire consistent imagery over reefs that would otherwise be expensive or a logistical challenge to survey.

Seafloor coverage data are typically derived from imagery through the application of a supervised image classification that assigns each pixel to the class to which it appears most spectrally similar. More recently, hyperspectral sensors have become available, which sample many narrow sections of the electromagnetic spectrum to provide a

*Email: shamylto@uow.edu.au

International Journal of Remote Sensing
ISSN 0143-1161 print/ISSN 1366-5901 online © 2011 Taylor & Francis
http://www.tandf.co.uk/journals
http://dx.doi.org/10.1080/01431161.2011.574162

contiguous coverage of radiance measurements across (Mather 2004). The many wavelengths that characterize a hyperspectral image introduce the possibility of employing analysis methods that treat data as continuous spectra, such as unmixing. Spectral unmixing techniques decompose the reflectance spectra of the materials with different properties inside the ground field of view of a single pixel (Kruse *et al*. 1993). They do so by mathematically inverting a composite spectrum as a means to determine the relative fractional contributions from its individual principal spectral components, or endmembers (Goodman and Ustin 2007).

The motivation of linear spectral unmixing focuses on defining the fractional components in the make-up of the pixel reflectance spectrum. The full hyperspectral data cube encompasses redundant information for a number of reasons, including the following:

(i) the underlying structure of hyperspectral reflectance curves in a given number of dimensions, λ_d, is almost always present at a dimension lower than d;
(ii) although there may be abundant functions available to solve an unmixing problem, the relevant structure in the solution space is limited by the number of endmember components present in each pixel;
(iii) the adjacent spectral bands in a remotely sensed image are generally correlated to each other and therefore yield similar estimates of benthic coverage in a linear equation; and
(iv) collinearity in spectral data (reflected by a nearly singular covariance matrix) adversely affects the interpretability of the coefficients of the linear model.

Hyperspectral images can therefore be usefully partitioned to eliminate the redundancy and encourage parsimonious representation of the reflectance features that are relevant for defining the fractional components of benthic coverages. A successful approach calls for a lower dimensional approximation to the covariance matrix. Multiple discriminant function analysis is presented as a statistical technique for the removal of structure in the correlation matrix of field-collected spectra to retain only key factors for operation with image data at the landscape scale. Advantages of dimension reduction include an increased signal-to-noise ratio for solution of the linear functions and reduced computer processing and storage burdens associated with spectrally and spatially rich data sets.

1.1 *Spectral unmixing of coral reef benthic assemblages*

In theory, an unmixing approach is particularly appropriate for application in a reef environment because the spatial scale of variability in the reef community (average coral size at the Wajh Barrier is approximately 30 cm^2) relative to the sensor resolution (1 m^2) is large. Mixing therefore occurs at the sensor (Campbell 1996). Several issues relating to the depth and turbidity of the water column above reef benthos confound the separation of spectra from different benthic components (Kutser *et al*. 2003). Furthermore, the dominant signal from sand, a high-albedo subpixel component, complicates signal integration into a single pixel value (Holden and Ledrew 2002). Nonetheless, the efficacy of linear spectral unmixing techniques has been evaluated for small-scale assemblages of coral reef substrata (<0.25 m^2) under ideal conditions, and results were found to benefit from a judicious choice of band locations (Hedley *et al*. 2004). Although the potential for unmixing homogenous coral reef communities has been demonstrated for Hyperion satellite imagery, the poor signal quality and large ground sampling distance has largely impaired the separation of similar

endmember spectra using imagery acquired from spaceborne platforms (Caras *et al.* 2008). Where diffuse attenuation coefficients are known, techniques comparable to classical spectral unmixing perform a Gaussian elimination for endmember quantities and solving the remaining function by successive approximation (Hedley and Mumby 2003). However, these techniques have been applied to coral reef spectra collected *in situ*, as opposed to image data. At the landscape scale, unmixing algorithms have been applied successfully to Airborne Visible/Infrared Imaging Spectrometer (AVIRIS) satellite imagery of reef environments using semi-analytical techniques (Goodman and Ustin 2007). These techniques simultaneously derive optical properties of the water column and bathymetry, which are subsequently used to transform endmember spectra from reflectance at the sea bottom to reflectance at the water surface. Although this approach was in close agreement with field data for shallow environments (80% overall accuracy at water depths <3 m), such semi-analytical and optimization techniques (see also Lee *et al*. 1998, 1999) are computationally intensive and expensive to implement.

An alternative practical approach is presented here for carrying out unmixing at the landscape scale on commercially available airborne hyperspectral data sets in a phased manner (figure 1). In the first phase, an optimal subset of wavelengths is defined for discriminating reef benthos that employs a combination of derivative and raw bands. This subset is then extracted for both field-collected and image spectra, which are brought into a common spectral frame of reference using standard pre-processing techniques that correct the airborne imagery for the effects of absorption and scattering in the atmosphere and water column. In the second phase, unmixing is applied to the image data to determine the relative abundance of reef benthos that are depicted

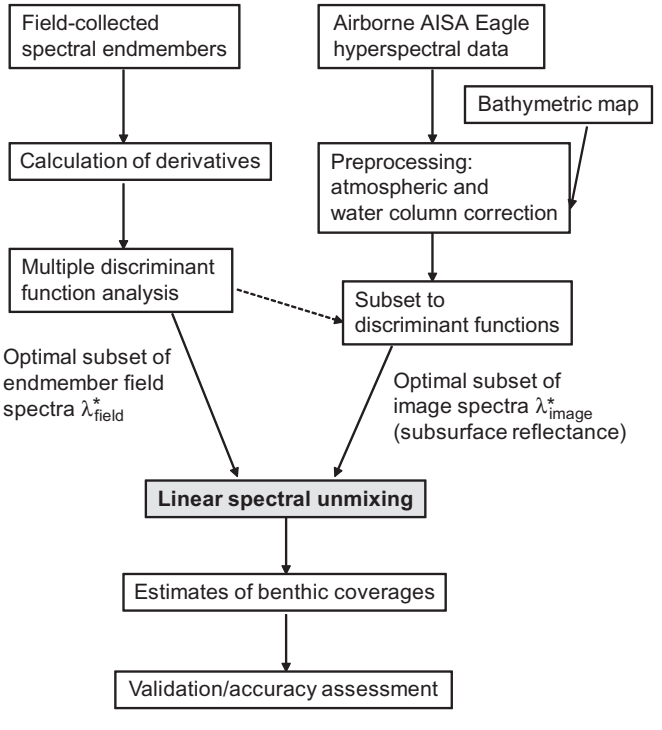

Figure 1. Overview of the staged spectral unmixing procedure.

in the hyperspectral imagery based on the characteristics of spectra collected *in situ*. The reflectance for each pixel of the image is assumed to be a linear combination of the reflectance of each material present within the pixel.

2. Methodology

2.1 *The study site*

The Al Wajh Bank is situated along the north-eastern part of the Red Sea coastline of the Kingdom of Saudi Arabia (figure 2). Inside the bank, a smaller area of image data was selected for application of the spectral unmixing algorithm. The area encompassed considerable variability in both reef form and the environmental gradients governing benthic community composition (e.g. areas were deep or shallow and exposed or sheltered to incident waves). There was also a range of community compositions present, making this sub-location adequate for the purpose of spectral unmixing.

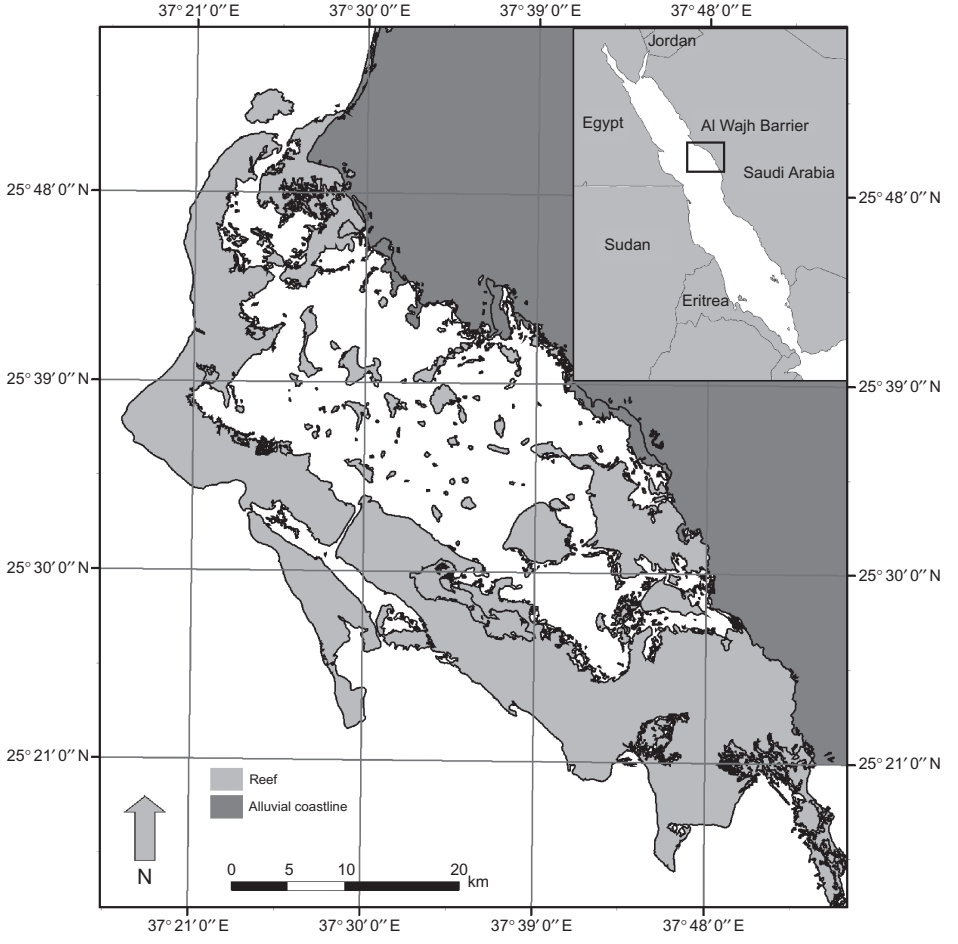

Figure 2. Location of the Al Wajh Bank, Saudi Arabia, Red Sea (25° 39′ N, 37° 35′ E).

Al Wajh comprises a north–south-aligned barrier reef stretching for around 100 km, separated by several narrow (<200 m width) channels (Sheppard *et al*. 1992). The outer edge of the system lies approximately 26 km offshore, running parallel to the shoreline for around 50 km, before changing course landward, at both its southern and northern limits, to enclose a central lagoon of area 1300 km^2. The depth of the enclosed lagoon platform ranges between 3 and 60 m, becoming progressively shallower towards the land. A range of islands and associated reef formations are supported on the shelf inside the barrier and a wide variety of benthic community types have developed under varying local environmental regimes associated with these (De Vantier 2000).

2.2 *Collection of spectral signatures of targets of interest: field spectroscopy*

Field spectra of a range of benthic assemblages were collected by a diver underwater using a RAMSES-ARC radiance sensor (TriOS Mess- und Datentechnik GmbH, Rastede, Germany). These spectra were used as input to the spectral unmixing algorithm. The spectrometer collected light in the wavelength range 300–920 nm, with an optical resolution of approximately 5 nm (TriOS 2004). The lens had a 7° field of view and was held at a distance of 10 cm from the target of interest to sample an area of approximately 42 cm^2. This was large enough to capture the internal spatial variability in radiance for benthic substrates, whilst ensuring that incoming radiance was sampled from the target of interest as opposed to adjacent objects. The head of the sensor was pointed downwards at an angle of 45° to the desired specimen. This enabled a diver operator to position his or herself in such a way as to avoid shadowing the target of interest and was in accordance with the established methods (e.g. Mazel 1996). Measurements were made with an integration time of 63 ms and five replications were collected for each benthic assemblage at each sample site. Signatures were collected for live coral, dead coral, macroalgae and carbonate sand. According to habitat maps previously prepared by the Japanese International Cooperation Agency using aerial photography, these benthic coverages were representative of all the community components falling inside the selected study area.

A white reference panel was used to estimate incident irradiance, which had a high and nearly constant reflectance over the visible region of the electromagnetic spectrum (Doxoran *et al.* 2002). Reflectance (R) was calculated as the ratio of spectral upwelling radiance (L_u) to downwelling (E_d) irradiance at a given wavelength. This assumed that both the panel and benthic surfaces reflected equally in all directions (i.e. were Lambertian reflectors):

$$R(\lambda) = \frac{L_u(\lambda)}{E_d(\lambda)}. \tag{1}$$

A white reference panel measurement was taken prior to each target measurement as close in time as was practical. This allowed a close approximation of incident irradiance to be derived for a given point in time. Radiance measurements were then converted to reflectance to adhere to the standard expression of optical properties. Endmember spectra were then averaged for each benthic target, prior to being smoothed to eliminate high-frequency noise. A Savitzky–Golay algorithm was used for smoothing, which performed a local polynomial regression on a series of values to determine the smoothed value for each point (Savitzky and Golay 1964). Following

smoothing, spectra were interpolated to yield reflectance at 1 nm intervals with a cubic spline (Karpouzli *et al*. 2004). This yielded spectrally a continuous data set for which derivatives could be calculated.

2.3 *Ground referencing: photo transects*

A series of six underwater validation transects were established across a range of inshore/offshore and sheltered/exposed locations on the Al Wajh Bank. A 20 m transect line was deployed, running parallel with the reef contour, at depths of 10 and 5 m. A diver swam along at a constant depth of 1 m above the line, taking photographs at 1 m intervals. This methodology yielded 20 photos per transect line, a total of 120 photographs, for subsequent coverage estimation using well-established line intercept transect methods (English *et al*. 1997).

2.4 *Image acquisition*

Hyperspectral data inside the Al Wajh barrier were acquired on 9 May 2008 using an aisaEAGLE imaging sensor (Spectral Imaging Ltd, Oulu, Finland) mounted to a Cessna seaplane. The flight line selected for unmixing was acquired from an altitude of 1520 m, producing a nominal pixel size of 1 m, and was located along the northern coast of the inner Wajh Barrier. The image covered approximately 20 km^2 (1.5 km wide by 13 km in length). The aisaEAGLE instrument measured 128 contiguous spectral bands from 400 to 994 nm at a spectral resolution of 5 nm. Although full spectral resolution was used in the pre-processing operations, all other analyses for the spectral unmixing utilized a reduced set of 26 bands from 400 to 900 nm (identified in figure 3).

2.5 *Image pre-processing (geometric correction, atmospheric correction)*

All image-processing operations were carried out using the software ENVI 4.5 (Environment for Visualising Images; ITT Visual Information Solutions, Boulder, CO, USA) with bespoke programming implemented through the associated IDL Workbench application. To provide for the accurate ($\pm$2.5 cm) georeferencing of the data, an integrated inertial navigation system (INS) was used during image acquisition coupled with a 12-channel differential global positioning system (dGPS) system. An internal geometry map (IGM) file was generated for the flight line to identify the easting and northing coordinate for each pixel. From this file, fully navigated imagery with the Universal Transverse Mercator (UTM) map projection, WGS-84 horizontal datum for UTM Zone 37 North, was generated.

An atmospheric correction was carried out using the Fast-Line-of-Sight Atmospheric Analysis of Spectral Hypercubes (FLAASH) module, which provided a physics-based derivation of atmospheric properties including surface pressure, water vapour column, aerosol and cloud overburdens. This was incorporated into a correction matrix for the purpose of inverting 'radiance at detector' measurements into 'radiance at water surface' values. The basis of the retrieval algorithm was strong correlation of the water vapour column amount to the ratio of reference (as measured at absorption band shoulders) and absorption (as measured at the centre of absorption bands) radiances. A Moderate Resolution Atmospheric Transmission (MODTRAN) model utilized a look-up table to generate water vapour on a pixel-by-pixel basis from surface radiance and the absorption radiance ratio over an expected range of water column and surface reflectance parameters (Cooley *et al*. 2002). Input parameters

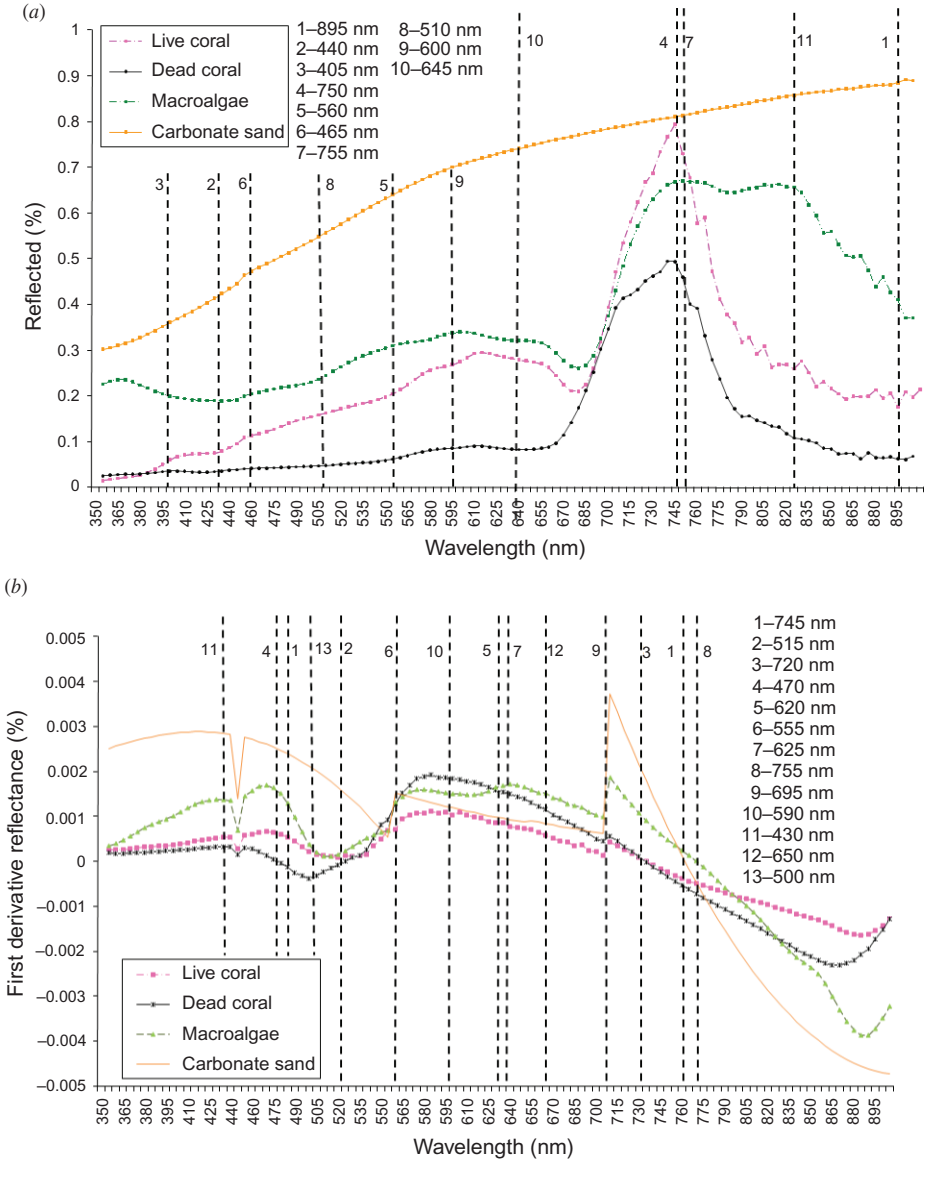

Figure 3. Mean (*a*) raw and (*b*) first-order derivative reflectance for each coastal community type sampled across the 110 bands of the TRIOS sensor. Discriminant functions are superimposed as dashed vertical lines onto the spectra.

including scene location, overpass time and date and sensor information (altitude, solar and viewing geometry) were used to generate water vapour look-up tables from staged water profiles for the flight strip. Standard water column amounts were calculated for a tropical atmosphere. Following atmospheric correction, the reflectance at 850 nm was subtracted from the atmospherically corrected imagery to account for any reflectance emanating directly from the water surface in the form of glint (Tassan 1992).

2.6 *Derivation of a bathymetric map from band ratio transformation*

Band ratio transformation methods were used to derive depth for each image pixel covering the study area. This approach was selected because it overcame the problem of mapping areas of variable albedo and has been found to accurately resolve the depth measurements for shallow structures such as coral pavement and algae. This method established a relationship between the changing ratio of two water-penetrating waveband pairs and water depth (Stumpf and Holderied 2003). If the linearized (natural logarithm) at-water reflectance (R_w) values of two image bands are plotted against each other, the ratio of the two (i.e. gradient) will vary with depth (z). This is due to the fact that as depth increases, reflectance of both bands will decrease; however, the reflectance of the longer wavelength band with higher absorption will decrease disproportionately faster than its shorter wavelength counterpart. Accordingly, the ratio of the green to blue reflectance will decrease. A change in bottom albedo will influence both bands to the same extent, thereby having no effect on the ratio (Philpot 1989). It is therefore possible to use pixels at known depths to scale the ratio of the two bands in order to approximate water depth from the reflectance of other pixels at the water surface, as per equation (2):

$$z = m_1 \frac{\ln\left(nR_w(\lambda_i)\right)}{\ln\left(nR_w(\lambda_j)\right)} - m_0, \tag{2}$$

where m_1 = a tunable constant to scale the image ratio to actual water depth; n = a fixed constant for all areas; and m_0 = the offset (y-intercept) for a depth of 0 m ($z = 0$).

This model was applied using atmospherically corrected reflectances for two bands, at green (550 nm) and blue (480 nm) wavelengths. In the first instance this was applied as an initial calibration step to data extracted from pixels of known depth (at 3, 5, 15 and 20 m) to establish values for m_0 and m_1. These depth readings were taken *in situ*, and corrected to a vertical datum of lowest astronomical tide. Coefficients m_0 and m_1 were determined from a plot of the ratio of linearized at-water reflectance ($\ln\lambda_i/\ln\lambda_j$) against depth as measured in the field. Once these had been established, equation (2) was applied across the remaining image pixels to derive a bathymetric model of the study area. The model was then validated against a set of 64 bathymetric records collected in the field.

2.7 *Image pre-processing (water column correction)*

The imagery was subjected to a water column correction method that can be summarized as follows: for each waveband, a diffuse attenuation coefficient (k) was established; a bathymetric map of the study area was created; terms for the correction of reflectance emanating from the water itself and refraction at the air/water surface were established; and at-feature radiance was calculated. The diffuse attenuation coefficient was estimated in the field by measuring incident irradiance along a vertical profile in the 300–900 nm region of the spectrum. An 'optically deep' area inside the Wajh lagoon was selected where there would be no signal from the seafloor. A pair of divers descended down a vertical drop line and five readings of irradiance were taken using the TriOS RAMSES-ARC hyperspectral sensor and a reflectance panel at depths of 5, 10, 15 and 20 m. Readings were then averaged for each depth and their natural logarithms plotted against depth for each waveband. The gradient of the

resultant line was taken to be the diffuse attenuation coefficient for that band (Green *et al*. 2000).

This model assumed uniform water quality throughout the scene and equal sky radiance from all directions. A band-wise water column correction method was carried out by inserting depth, deep-water reflectance and attenuation information into equation (4), which was derived from equation (3) (Bierworth *et al*. 1993):

$$R_z = R_x e^{-2kz}, \tag{3}$$

from which we can derive

$$R_x = \frac{\frac{1}{0.54}\ R_z - \left(1 - e^{-2kz}\right)\ R_w}{e^{-2kz}}, \tag{4}$$

where R_z = reflectance at the water surface, R_x = at-feature reflectance, k = diffuse attenuation coefficient, z = depth and R_w = deep-water reflectance.

Following calculation of the diffuse attenuation coefficient and depth on a per pixel basis, the model maker function of ERDAS IMAGINE software (ERDAS Inc., Norcross, GA, USA) was used in a stepwise manner to calculate at-feature radiance. To implement equation (3), the result of this step was multiplied by 1/0.54 to account for refraction at the air/water surface boundary. To correct for the effects of scattering in the water column, statistics from a series of 500 deep-water pixels were then exported and the mean reflectance was measured for each individual band and, combined with the bathymetric map, multiplied by the result of $1 - e^{-2kz}$ (as calculated from the bathymetric map and diffuse attenuation coefficients). Finally, to estimate at-feature radiance, the result of this step was taken from the atmospherically corrected imagery layer, which had previously been adjusted for surface reflectance and refraction, and divided by e^{-2kz}.

2.8 *Selection of an appropriate band set: derivative and multiple discriminant function analysis*

An optimal subset of wavelengths for resolving the reflectance of key benthic coverages was identified by calculating the derivatives of spectra collected in the field and applying multiple discriminant function analysis to both raw and first derivative spectra. Derivative functions of each spectrum gave an indication of rate of change or slope of the original spectrum as input into the discriminant function model. Waveband first-order derivatives were calculated using the derivatives' computation tool from the Spectral Analysis and Management System (equation (5)) (Rueda and Wrona 2003). This calculated a derivative, d′, by taking the first discrete derivative of the previous band:

$$d'(R_x) = \frac{d\,(R_{x+1}) - d\,(R_x)}{\lambda_{x+1} - \lambda_x}, \tag{5}$$

where $d'(R_x)$ = discrete derivative of reflectance in band x, $d(R_x)$ = discrete reflectance value at band x, $d(R_{x+1})$ = discrete reflectance value at band $x + 1$, λ_x = wavelength of band x and λ_{x+1} = wavelength of band $x + 1$.

The discriminant function analysis was performed using SPSS software (IBM, Armonk, NY, USA) and carried out on the reflectance spectra and their first derivatives. Radiance data across 128 wavebands for 140 cases were grouped into four types of benthic assemblage in matrix notation. To build a model of discrimination, individual wavelengths were chosen by a forward stepwise selection process based on calculations of their respective p-values resulting from successive multivariate partial-F tests ($p < 0.05$). This stepwise process continually added new wavelengths into the selection until variation between the groups was no longer maximized. The discriminant (or canonical) functions were calculated as linear combinations of the wavelengths or bands that best separated the classes (Hamylton 2009).

2.9 *Image classification: spectral unmixing*

Average field spectra for the four different endmembers were input into the unmixing algorithm. To allow comparison between the field and image spectra, image data were converted from radiance to reflectance by dividing each band by the corresponding radiance of a large white target that was deployed on the ground in the sensor field of view during image acquisition. Although a subset of the full spectral range was chosen, the requirement of there being more bands than mixing endmembers was met.

Derivatives were amenable to use in linear mixture modelling because they met the requirement that the derivative of the sum of two or more spectra was equal to the derivatives of the individual spectra summed (equation (6)):

$$\frac{\mathrm{d}(x+y)}{\mathrm{d}\lambda} = \frac{\mathrm{d}x}{\mathrm{d}\lambda} + \frac{\mathrm{d}y}{\mathrm{d}\lambda}. \tag{6}$$

Furthermore, for a hybrid subset comprising both derivative and raw bands, the total reflectance was equal to the sum of the individual spectra, both raw and derivative, and could therefore be treated as a linear model. Linear mixture models assume that light photons reflecting off the target of interest do not interact with other ground surface objects, and that for a given wavelength, the total number of photons reflected from a single pixel and detected by the sensor can be described as a linear function of the reflectance of the individual components and the fractional area of the pixels they cover (equation (7)) (Schowengerdt 1997):

$$R_x = \sum_{j=1}^{n} a_{xj} f_j + e_x, \tag{7}$$

where R_x = reflectance of a given pixel in the xth of z spectral bands, n = the number of mixture components, f_j = the jth fractional component in the make-up of R_x, a_{xj} = the reflectance of mixture component j in spectral band x and e_x = the difference between the measured pixel reflectance and that computed from the model.

This expresses the idea that, given n cover types within the pixel, the integrated signal received at the sensor in a given band will be the linear sum of the individual interactions (Mather 2004). Thus, for a benthic composition of four coverages inside each pixel, each with known reflectance from the field spectra, a set of simultaneous linear equations was solved to derive the proportions of the individual elements

falling inside each pixel. Output from the unmixing process was several images showing the derived spatial patterns of abundance for each benthic coverage type (Kruse *et al*. 1993).

2.10 *Validation of reef community coverage components*

Classification accuracy was assessed using a combination of the root mean square error model, which was generated as part of the spectral unmixing process (Cooley *et al*. 2002), and the field data collected using photo transects. Two transects, one shallow (5 m depth) and one deep (10 m depth), were sampled at each location, yielding a total of 12 validation cases for each benthic coverage. Data from the photo transects were overlaid onto the coral cover map and compared to figures collected directly in the field. Due to the difficulty of exactly matching the location of surveys in the field to pixels on the image, coverage statistics were averaged across an area that included a 1 m border around the immediate overlay location and a single value was compared for each transect.

The accuracy of benthic coverage estimations was assessed by means of a linear regression between the actual proportion (as recorded by the photo transect) and the estimated proportion (from spectral unmixing). Linear regression was chosen because it has a tangible meaning (i.e. the amount of variation in the distribution of the benthic coverage inside the study area explained by the unmixing results) and encompassed both thematic and locational aspects of accuracy.

3. Results

3.1 *Representation of benthic coverages: field stage*

Two hundred and fifty reflectance spectra were collected in total. Overall, there was high variability between the spectra of the different benthic coverages, which each had their own unique reflectance curve shape. This indicated the suitability of this region of the electromagnetic spectrum for resolving the different coverages. The sand spectra had the highest reflectance values and the least variation in shape. A dip around the 658–662 nm region and a peak around 696 nm was characteristic of the 'red edge' of photosynthetic organisms that utilize chlorophyll-*a*, which was apparent in the live coral, dead coral and macroalgae spectra (figure 3(*a*)).

To adequately separate out the coverages, the data set was reduced from 128 bands to 24 discriminant functions composed of raw reflectance and first-order derivative spectra, as identified by the multiple discriminant function analysis. Of the discriminant functions identified, 11 were raw data wavebands and 13 were first-order derivative functions. These ranged between 405 and 895 nm for the raw reflectance spectra and 430 and 795 nm for the first derivative spectra; within these ranges, discriminant functions appeared to be evenly spaced (figure 3). Although a few of the selected bands were at wavelengths known to be influenced by absorption in the water column (i.e. > 700 nm), many of the coral communities inside the Al Wajh lagoon were situated on a shallow platform, which meant that they were close to the water surface. Bands in these wavelengths therefore retained useful information for the unmixing algorithm.

A high-quality image of the study area was acquired, which was relatively free of the effects caused by glint on the water surface, cloud cover and the bidirectional

reflectance function. The bathymetric map provided as input to the water column correction algorithm produced using band ratio methods showed a close correlation to depth records collected directly in the field ($R^2 = 0.87$).

A number of different reef structures fell inside the study area, which can be summarized as three morphological units. These were (i) an exposed platform to the east, with a shallow shelf to the west within the northern section of the study area; this was separated by a deep channel (a major passage of water exchange at the northern end of the lagoon) from (ii) a large submerged ridge network running from east to west bisecting the centre of the study area, with (iii) a series of patch reefs on a shallow (<5–10 m) shelf to the south. The 12 underwater photo transects revealed a wide variation in the coral community composition at the different depths surveyed on these morphological features (figure 4).

Figure 5 illustrates the spatial distribution of spectrally unmixed estimates for each benthic coverage, along with a colour composite of the image for reference and the bathymetric model generated. The linear mixture model estimated a high cover of live coral associated with the three morphological units, that is, to the north of the study area around the shallow platform, covering a dominant proportion of the ridge network and in conjunction with the patches in the south of the study site. Mean live coral cover across the whole study areas was 35.13% (standard deviation 17.6).

Dead coral occupied the shallower areas of these reef structures, with high coverage along the tops of several prominent ridges among the network across the centre of the study site and the exposed platform to the north-east. Mean dead coral cover was 49.41% (standard deviation 22.1).

Mean macroalgal cover was 51.76% (standard deviation 37.8). A macroalgal mat seemed to have formed over a large area of the lagoon floor, particularly in flat areas

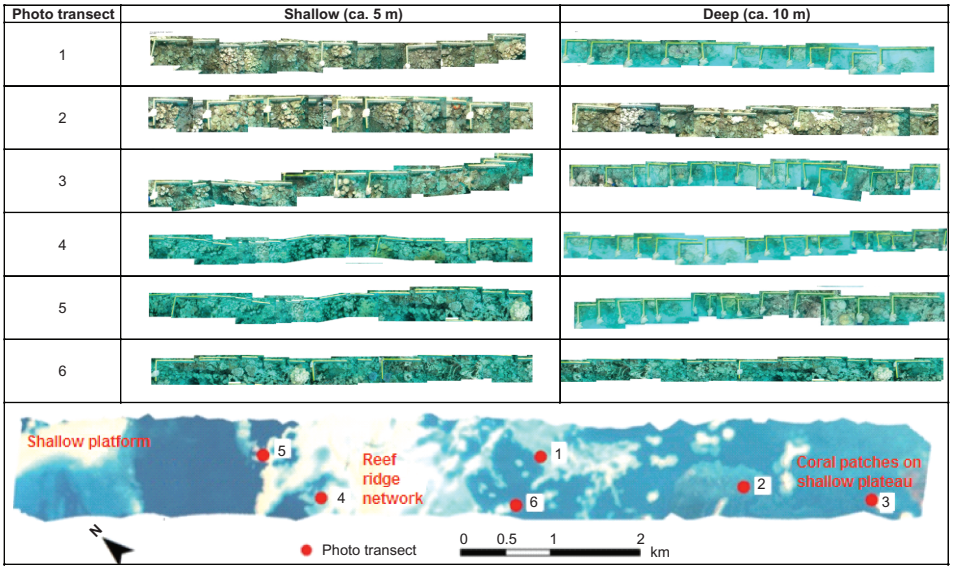

Figure 4. Photo transects used for validating hard coral cover estimations derived from the spectral unmixing algorithm, one shallow and one deep transect per site. Locations plotted on the RGB image composite of the study area.

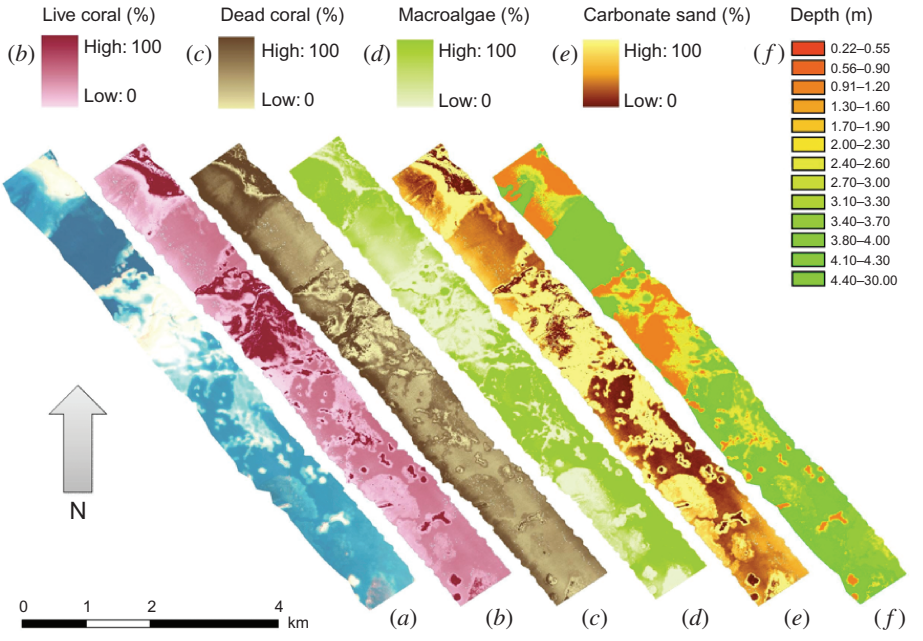

Figure 5. (*a*) Raw three-band (R, G, B) image composite of the study area for comparison. Spectrally unmixed coverages of (*b*) live coral, (*c*) dead coral, (*d*) macroalgae, (*e*) carbonate sand and (*f*) bathymetric map of the study area.

towards the south of the study area. There was a limited coverage of macroalgae evident in areas where reefs were well developed, that is, around the ridge network in the centre of the study site and in association with reef patches.

Carbonate sand occurred in association with the reefs and appeared to be at particularly high proportions in areas directly adjacent to coral, that is, in rings around the reef patches on the shallow shelf to the south of the study area. Mean carbonate sand cover was 36.61% (standard deviation 36.2).

The bathymetric map revealed a deep channel towards the north of the study area. In the broader context of the Wajh Barrier, this leads to a large opening in the northern barrier wall, one of the only two sites of water exchange between the lagoon and outside ocean waters. The shallower areas of the study site coincided with the platform in the north, the ridge network and the tops of the patches in the south. Water depths inside the overall study area ranged between 0.2 m above reef patches and 30 m inside the channel towards the northern end of the study area, although a large portion of the southern extent of the study area was on a shallow platform (<5 m water depth).

3.2 *Validation of reef community coverage components*

The overall root mean square error (i.e. the difference between the measured pixel reflectance and the mixture model function computed for each pixel, denoted by the e_x term in equation (7)) estimated by the unmixing algorithm was low (<0.001). R^2 ranged between 0.71 and 0.89, suggesting a high correspondence of the modelled live coral cover values with those measured in the field (figure 6).

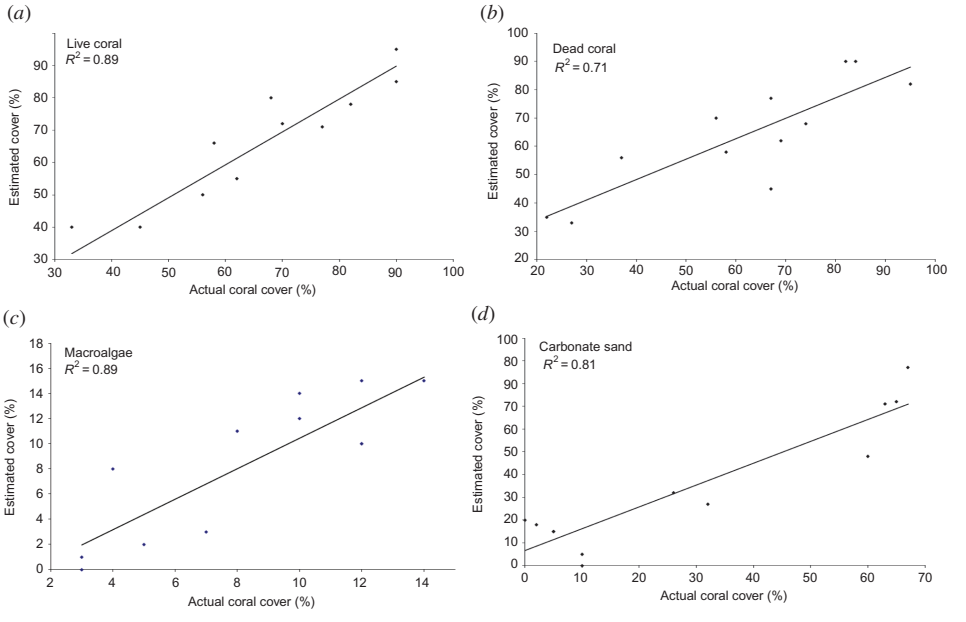

Figure 6. Actual (as measured in the field) against estimated (from the unmixing model) cover for each of the benthic coverages: (*a*) live coral, (*b*) dead coral, (*c*) macroalgae and (*d*) carbonate sand.

4. Discussion

Spectral unmixing offers a fundamentally different habitat map product to a conventional per-pixel classification. A per-pixel classification generates a single habitat map that identifies the dominant benthic component inside each pixel's field of view in accordance with its overall spectral properties, whereas an unmixing classification generates several maps depicting the relative contribution from each benthic component inside the study area. Individually, each of these maps illustrate the distribution of a single component of the reef community, while together they represent the overall habitat composition. Advantages of the latter map product include (i) a more realistic representation of habitat coverage due to the removal of generalization for subpixel components (i.e. presence/absence vs. fractional components); (ii) production of a series of habitat maps at a higher measurement level (i.e. nominal vs. ratio), which lends more versatility for subsequent analysis, for example, in modelling applications; and (iii) greater opportunities to focus on particular benthic components of interest given the development of a single map for each input spectrum. These advantages have clear utility for management activities such as estimating the distribution and coverage of individual components for community status assessment and assessing change in this status over time.

Collectively, the series of maps invites coastal managers to consider the geography of coverage dynamics that are relevant to conservation and protection strategies. For example, the presence of dead coral framework liberates space for the settlement of macroalgae, which dominates further by inhibiting coral recruitment, fecundity and growth because of competition for space and light. Thus, macroalgae form stable communities that resist a return to coral domination and phase changes occur between

stable equilibria (Done 1992). Transitions between such equilibria are often responses to perturbations at the landscape scale (Knowlton 1992). It follows that a comparison of the unmixed maps that represent the coverage of macroalgae, live coral and dead coral might reveal locations where such equilibria have been reached, as would be characterized by both macroalgae and dead coral in high proportions, combined with live coral in low proportions. The shallow shelf to the north-west of the study area exemplifies this combination, for which available field data support the assertion that a phase change has occurred.

In contrast, those areas where live coral is the dominant benthic coverage present themselves as candidate sites for conservation. Identification and subsequent protection of these areas is particularly important given the value of Scleractinia (reef building corals) as keystone species in tropical coastal systems due to their functional role as primary producers, community calcifiers, dissipators of incident wave energy and providers of structural rugosity (Moberg and Folke 1999). In this study, these emerge in association with the reef morphological units, that is, the shallow platform to the north, the ridge network to the centre and the patches to the south of the study area.

Furthermore, comparison of coverages may in some instances provide insight on causal processes underpinning the spatial distributions revealed. A key objective of studying shallow marine landscapes is the identification and quantification of spatially realistic relationships between functional system properties and the structural form of shallow water communities. Treatment of the output maps as representations of structural responses might uncover relationships between variables that summarize some aspects of the landscape form and those that represent potential functional drivers (Mather 1979). For example, the notably high coverage of carbonate sand around live coral patches on the shallow platform towards the south of the study area stands in contrast to the relative dearth of macroalgae in these locations. It may be that localized grazing associated with the territorial behaviour of damselfish (Pomacentridae) or urchins (*Diadema antillarum*) inhabiting these patches has given rise to these patterns (Hay 1981, Ormond *et al.* 1996). It is through a comparison of the different coverage distributions that such patterns become evident.

5. Conclusions

This study has demonstrated a successful staged approach for deriving the spatial distribution of benthic coverages (live coral, dead coral, macroalgae and sand) inside the Al Wajh Bank using linear spectral unmixing analysis. The model was able to unmix subpixel composition of four reef community benthic coverages accurately, with correlation coefficients > 0.71 between the actual and estimated class proportions in all cases. Such close agreement against available field data was achieved from an unmixing analysis that employed an optimally placed subset composed of 24 hybrid raw and first derivative bands. The practicality of this phased approach lies in efficient use of the spectrally continuous information available through the calculation of derivatives, combined with the identification of an optimal subset of bands for solving the unmixing equation while simultaneously lowering the computational image-processing burdens. These results provide a significant advance on (i) standard pixel-based single substratum classifications and (ii) previous attempts to unmix the composition of benthic communities that have been applied at much smaller scales or used prohibitively intensive methodologies. This latter advance is likely to be due to the enhanced spatial and spectral resolution of the aisaEAGLE sensor.

The success of this unmixing approach implies promise for users of hyperspectral imagery to employ coarser spatial resolution imagery for underwater applications. This could result in further advantages relating to image storage space and cost, and particularly with respect to time invested in overcoming the pre-processing challenges associated with the presence of a water column.

This research demonstrates that some of the more recent advances in remote sensing, that is, the enhanced spectral detail available from hyperspectral instruments, can be utilized in a practical and cost-effective manner to generate estimates of the distribution of the various components that make-up coral reef communities. In turn, this represents a valuable tool for the systematic mapping, evaluation and monitoring of coral reef communities at the landscape scale.

Acknowledgements

This work would not have been possible without the generous support of the Khaled bin Sultan Living Oceans Foundation. Dr Tom Spencer at the University of Cambridge is thanked for guidance on the manuscript and Dr Rainer Reuter, University of Oldenburg, is thanked for assistance with fieldwork.

References

Bierworth, P.N., Lee, T.J. and Burne, R.V., 1993, Shallow sea-floor reflectance and water depth derived by unmixing multispectral imagery. *Photogrammetric Engineering and Remote Sensing*, **59**, pp. 331–338.

Campbell, J.B., 1996, *Introduction to Remote Sensing*, 2nd ed. (London: Taylor & Francis Ltd.).

Caras, T., Karnieli, A., Bendor, E. and Meaden, G., 2008, Investigating the potential of monitoring coral reefs using unmixing of spaceborne hyperspectral imagery. In *Proceedings of the 11th International Coral Reef Symposium*, Fort Lauderdale, FL (Fort Lauderdale, FL: International Coral Reef Society).

Cooley, T., Anderson, G.P., Felde, G.W., Hoke, M.L., Ratowski, A.J., Chetwynd, J.H., Gardner, J.A., Adler-Golden, SM., Matthew, M.W., Bernstein, L.S., Achara, P.K., Miller, D. and Lewis, P., 2002, FLAASH: a MODTRAN4-based atmospheric correction algorithm, its application and validation. In *Proceedings of the IEEE Symposium on Geoscience and Remote Sensing*, 8–11 July 2002 (College Park, MD: IEEE Xplore).

De Vantier, L., 2000, Final report on the study on coastal/marine habitats and biological inventories in the northern part of the Red Sea coast in the Kingdom of Saudi Arabia. Unpublished report to the National Commission for Wildlife Conservation and Development, Riyadh, Saudi Arabia. Japan International Cooperation Agency.

Done, T.J., 1992, Phase shifts in coral reef communities and their ecological significance. *Hydrobiologia*, **247**, pp. 121–132.

Doxoran, D., Froidefond, J., Lavendar, S. and Castaing, P., 2002, Spectral signature of highly turbid waters; application with SPOT data to quantify suspended particulate matter concentrations. *Remote Sensing of Environment*, **81**, pp. 149–161.

English, S., Wilkinson, C.R. and Baker, V., 1997, *Survey Manual for Tropical Marine Resources* (Townsville, QLD: Australian Institute of Marine Sciences).

Goodman, J.A. and Ustin, S.L., 2007, Classification of benthic composition in a coral reef environment using spectral unmixing. *Journal of Applied Remote Sensing*, **1**, pp. 1–16.

GREEN, E.P., MUMBY, P.J., EDWARDS, A.J. and CLARK, C.D., 2000, *Remote Sensing Handbook for Tropical Coastal Management*, 316 pp. (Paris: UNESCO Publishing).

HAMYLTON, S., 2009, Determination of the separability of coastal community assemblages of the Al Wajh Barrier Reef, Red Sea, from hyperspectral data. *Central European Journal of Geosciences*, **1**, pp. 95–105.

HAY, M.E., 1981, Spatial patterns of grazing intensity on a Caribbean barrier reef: herbivory and algal distribution. *Aquatic Botany*, **11**, pp. 97–109.

HEDLEY, J.D. and MUMBY, P.J., 2003, A remote sensing method for resolving depth and subpixel composition of aquatic benthos. *Limnology and Oceanography*, **48**, pp. 480–488.

HEDLEY, J.D., MUMBY, P.J., JOYCE, E. and PHINN, S., 2004, Spectral unmixing of coral reef benthos under ideal conditions. *Coral Reefs*, **23**, pp. 60–73.

HOLDEN, H. and LEDREW, E., 2002, Hyperspectral linear mixing based on in situ measurements in a coral reef environment. In *International Geoscience and Remote Sensing Symposium*, 24–28 June 2002, Toronto, ON, Canada (Sydney: IGARSS).

KARPOUZLI, E., MALTHIUS, T.J.M. and PLACE, C.J., 2004, Hyperspectral discrimination of coral reef benthic communities in the western Caribbean. *Coral Reefs*, **24**, pp. 124–134.

KNOWLTON, N., 1992, Thresholds and multiple stable states in coral reef community dynamics. *American Zoologist*, **32**, pp. 674–682.

KRUSE, F.A., LEFKOFF, A.B., BOARDMAN, J.B., HEIDEBRECHT, K.B., SHAPIRO, A.T., BARLOON, P.J. and GOETZ, A.F.H., 1993, The spectral image processing system (SIPS) – interactive visualization and analysis of imaging spectrometer data. *Remote Sensing of the Environment*, **44**, pp. 145–163.

KUTSER, T., DEKKER, A.G. and SKIRVING, W., 2003, Modelling spectral discrimination of Great Barrier Reef benthic communities by remote sensing instruments. *Limnology and Oceanography*, **48**, pp. 497–510.

LEE, Z.P., CARDER, K.L., MOBLEY, C.D., STEWARD, R.G. and PATCH, J.S., 1998, Hyperspectral remote sensing for shallow waters. 1. A semianalytical model. *Applied Optics*, **37**, pp. 6329–6338.

LEE, Z.P., CARDER, K.L., MOBLEY, C.D., STEWARD, R.G. and PATCH, J.S., 1999, Hyperspectral remote sensing for shallow waters: 2. Deriving bottom depths and water properties by optimization. *Applied Optics*, **38**, pp. 3831–3843.

MATHER, P.M., 1979, Theory and quantitative methods in geomorphology. *Progress in Physical Geography*, **3**, pp. 471–487.

MATHER, P.M., 2004, *Computer Processing of Remotely Sensed Images: An Introduction*, 2nd ed. (Chichester, UK: John Wiley & Sons).

MAZEL, C.H., 1996, Coral fluorescence characteristics: excitation-emission spectra, fluorescence efficiencies, and contribution to apparent reflectance. In *Ocean Optics XIII, Proceedings of SPIE*, 8–11 July, Halifax, NS, Canada, Vol. 2983, pp. 240–245.

MOBERG, F. and FOLKE, C., 1999, Ecological goods and services of coral reef ecosystems. *Ecological Economics*, **29**, pp. 215–233.

ORMOND, R.F.G., ROBERTS, J.M. and JAN, R.Q., 1996, Behavioural differences in microhabitat use by damselfishes (Pomacentridae): implications for reef fish biodiversity. *Journal of Experimental Marine Biology and Ecology*, **202**, pp. 85–95.

PHILPOT, W.D., 1989, Bathymetric mapping with passive multispectral imagery. *Applied Optics*, **28**, pp. 1569–1578.

RUEDA, C.A. and WRONA, A.F., 2003, *Spectral Analysis and Management System, Version 2, User's Manual, Centre for Spatial Technologies and Remote Sensing* (Davis, CA: University of California).

SAVITZKY, A. and GOLAY, M.J.E., 1964, Smoothing and differentiation of data by simplified least squares procedures. *Analytical Chemistry*, **36**, pp. 1627–1639.

SCHOWENGERDT, R.A., 1997, *Remote Sensing: Models and Methods for Image Processing*, 2nd ed. (London: Academic Press).

Sheppard, C.R.C., Price, A. and Roberts, C., 1992, *Marine Ecology of the Arabian Region: Patterns and Processes in Extreme Tropical Environments*, pp. 1–359 (London: Academic Press).

Stumpf, R.P. and Holderied, K., 2003, Determination of water depth with high-resolution satellite imagery over variable bottom types. *Limnology and Oceanography*, **48**, pp. 547–556.

Tassan, S., 1992, An algorithm for the identification of benthic algae in the Venice lagoon from Thematic Mapper data. *International Journal of Remote Sensing*, **13**, pp. 2887–2909.

TriOS, 2004, *Ramses Hyperspectral Radiometer Manual Release* 1.0, 27 pp.